NANO LETTERS

Letter

pubs.acs.org/NanoLett

Large-Area Nanosquare Arrays from Shear-Aligned Block Copolymer Thin Films

So Youn Kim,[†,‡] Adam Nunns,[§] Jessica Gwyther,[§] Raleigh L. Davis,[†] Ian Manners,[§] Paul M. Chaikin,[∥] and Richard A. Register*[,†]

[†]Department of Chemical and Biological Engineering, Princeton University, Princeton, New Jersey 08544, United States

[‡]School of Energy and Chemical Engineering, Ulsan National Institute of Science and Technology, Ulsan, South Korea

[§]School of Chemistry, University of Bristol, Bristol BS8 1TS, United Kingdom

[∥]Department of Physics, New York University, 4 Washington Place, New York, New York 10003, United States

Supporting Information

ABSTRACT: While block copolymer lithography has been broadly applied as a bottom-up patterning technique, only a few nanopattern symmetries, such as hexagonally packed dots or parallel stripes, can be produced by spontaneous self-assembly of simple diblock copolymers; even a simple square packing has heretofore required more intricate macromolecular architectures or nanoscale substrate prepatterning. In this study, we demonstrate that square, rectangular, and rhombic arrays can be created via shear-alignment of distinct layers of cylinder-forming block copolymers, coupled with cross-linking of the layers using ultraviolet light. Furthermore, these block copolymer arrays can in turn be used as templates to fabricate dense, substrate-supported arrays of nanostructures comprising a wide variety of elements: deep (>50 nm) nanowells, nanoposts, and thin metal nanodots (3 nm thick, 35 nm pitch) are all demonstrated.

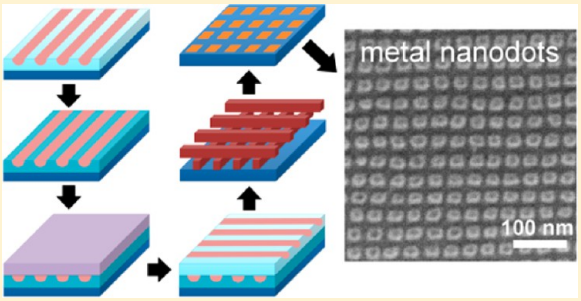

KEYWORDS: *Block copolymer lithography, nanopatterning, square arrays, metal dots*

At sufficiently high values of the Flory interaction parameter (χ) and degree of polymerization (N), block copolymers can form regular nanoscale morphologies, whose symmetry is determined principally by the volume fraction of each block; the characteristic dimensions of these structures are easily controllable over the range of 10−100 nm by varying N. This ability to create dense periodic patterns extends to thin films, where block copolymers have been highlighted in nanolithographic applications expected to provide fine resolution and scalability.[1−3] While many techniques,[4] such as graphoepitaxy, surface chemical patterning, and shearing,[5] can impart long-range order to the nanostructures in block copolymer thin films, only a few symmetries have been demonstrated in such arrays:[1,4] periodic stripes can be created from cylindrical- or lamellar-phase block copolymers, while hexagonally packed arrays of dots can be formed from spherical- or cylindrical-phase block copolymers. These hexagonal arrays have been used as templates for the fabrication of high density arrays of quantum dots,[6−8] standing nanowires,[9] magnetic storage media,[10] flash memory devices,[3] semiconductor capacitors,[11] and contact holes.[12] In some applications, there is strong interest in using square or rectangular arrays instead, because these are more compatible with semiconductor integrated circuit design standards;[3,13,14] however, creating square or rectangular patterns, which do not form by unguided self-assembly of simple diblock copolymers, remains a challenge.[14]

One route to achieving square lattices has been to introduce more complex macromolecular architectures. So-called "non-frustrated" ABC triblock copolymers, wherein the χ value between A and C is larger than between B and either A or C, can form a tetragonally packed arrangement of distinct A and C cylinders, provided the volume fractions of the end blocks are such that they each form cylinders (∼0.20);[15] perpendicular to the cylinder axis, either the A or C sublattice thus shows a square packing. Son et al. have applied this idea to thin films, wherein the cylinders are induced to stand perpendicular to the substrate by a suitable surface treatment and have employed such films for pattern transfer.[16] Tang et al. showed that a similar tetragonal lattice could be obtained in thin films with a judiciously chosen blend of AB and B′C diblock copolymers, where the B and B′ blocks strongly hydrogen bond to each other.[17] However, this macromolecular engineering approach places substantial constraints on the interblock interactions and thus on the chemistries of the blocks that may be employed in the materials. Moreover, these films still formed a polygrain structure with grain sizes on the order of a few microns; achieving order over longer ranges, or alignment of the lattice

Received: June 27, 2014
Revised: July 23, 2014
Published: September 11, 2014

   dx.doi.org/10.1021/nl502416b | *Nano Lett.* 2014, 14, 5698−5705

Scheme 1. Schematic Process Flow for the Fabrication of Nano-Square Arrays from Block Copolymers[a]

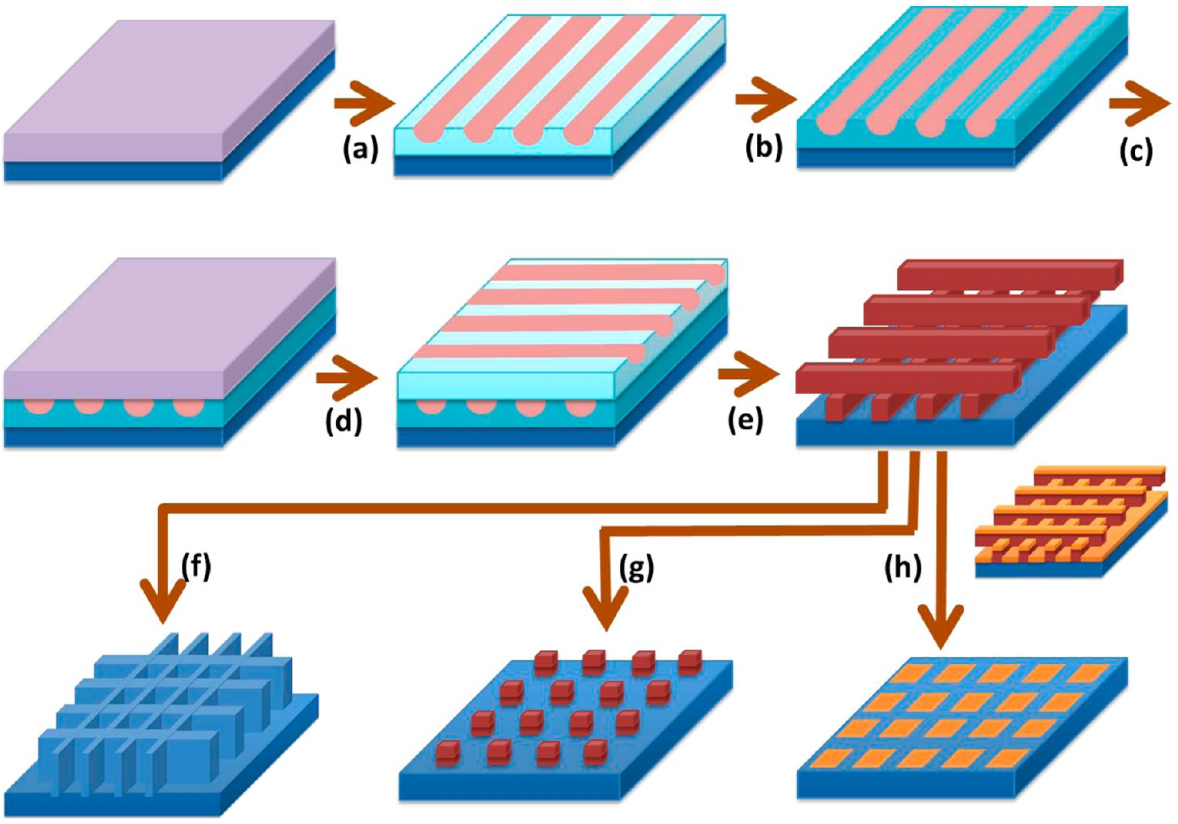

[a](a) Shear alignment of the spin-coated first layer, (b) UV irradiation, (c) spin-coating of the second layer, (d) second shear alignment orthogonal to the first shear direction, (e) removal of matrix block by RIE, (f) deep Si etching to create square nanowells, (g) controlled wet etching to create a square array of nanoposts, and (h) metal evaporation and lift-off to create metal nanodot arrays. Hemicylinders, as formed by PS-PFiPMS 36-15, are shown above; the process flow is analogous for the full cylinders formed by PS-PFEMS 27-11 and PS-PHMA 33-78.

in a particular direction, required nanoscale prepatterning of the substrate by electron-beam (e-beam) lithography.[16]

Alternatively, one can create square or rectangular arrays in simple diblock copolymer films through e-beam or X-ray interference lithographic prepatterning of the substrate, by generating a chemical pattern wherein the different blocks selectively wet the chemically dissimilar areas;[18−21] in this case, the block copolymer's function is to perfect and amplify the pattern, not to generate the pattern, which must be written separately. The required substrate prepatterning limits the size of the arrays which can be fabricated, typically to a few tens of micrometers. Rectangular lattices may also be created by superimposing two striped patterns; this has also been achieved using block copolymers following this same chemical templating approach,[22,23] though the required substrate prepatterning by e-beam lithography is still an impediment to large-area fabrication. Alternatively, striped patterns covering large areas may be obtained by shear-alignment of block copolymer thin films.[5,24−28] Jeong et al. superimposed two such patterns created from a polystyrene-poly(dimethylsiloxane) diblock (PS-PDMS) by etching the first layer with oxygen plasma, then coating, shearing, and etching a second layer.[29] However, the topography present after etching the first layer hampered alignment of the second layer, leading to a high density of defects in the final array.

In this study, we demonstrate the generation of nanoscale square patterns over large (cm^2) areas, using cylinder-forming block copolymers aligned in a cross-pattern, following the process flow shown in Scheme 1. The cross-pattern is created from two layers of cylinder-forming block copolymers, where each layer is spin-coated and shear-aligned sequentially. After the first block copolymer layer is shear-aligned (step a), the film structure is fixed by UV irradiation (step b); the second block copolymer layer is then spin-coated (step c) and shear-aligned in the orthogonal direction (step d). Reactive ion etching (RIE) is then used to selectively remove the matrix polymer surrounding the cylinders in both layers simultaneously (step e), yielding a double-layered cross-bar pattern that serves as a template for square arrays, whose elements can consist of square wells (step f), a square lattice of dots at the intersection points of the cross-pattern (step g), or complementary square dots between the stripes in the cross-bars (step h).

In the first example, a polystyrene-poly(ferrocenylisopropylmethylsilane) diblock copolymer, PS-PFiPMS 36-15, with PS and PFiPMS blocks having number-average molecular weights of 36 and 15 kg/mol, was employed to create the cross-bar pattern. A spin-coated film of PS-PFiPMS 36-15 (19 nm thick) was first aligned by applying 17 kPa of shear stress over a 1.3 × 1.3 cm^2 area with a cured poly(dimethylsiloxane) pad at 150 °C, well above the glass transition temperatures of both blocks. At the thickness of 19 nm, PS-PFiPMS 36-15 forms a layer of hemicylinders of PFiPMS, wherein both PS and PFiPMS are exposed at the film surface; these hemicylinders can be shear-aligned.[26] Figure 1a shows a tapping-mode atomic force microscopy (AFM) image revealing the film structure prior to shear. After shear

dx.doi.org/10.1021/nl502416b | Nano Lett. 2014, 14, 5698−5705

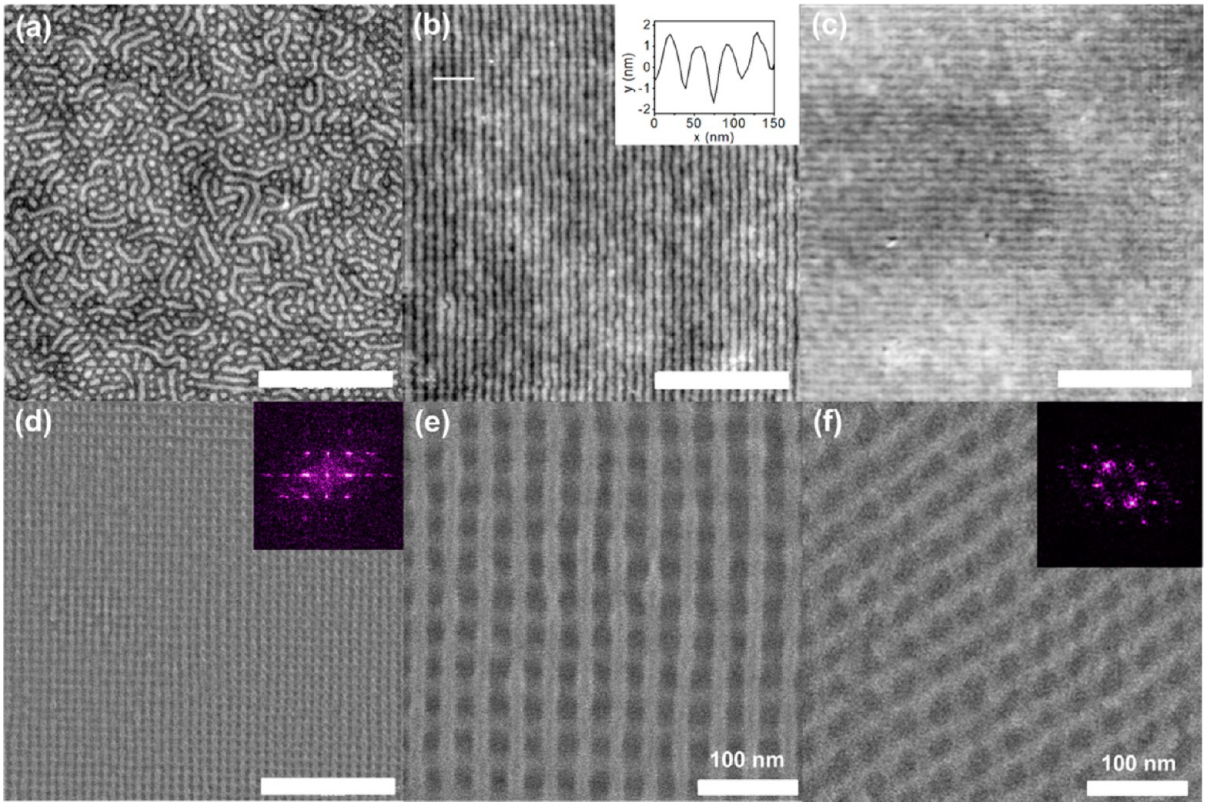

Figure 1. Images taken at various steps in the process flow. (a) AFM height image of a spin-coated but unsheared film of PS-PFiPMS 36-15 (19 nm thick) following 30 min of thermal annealing with subsequent UV treatment to enhance the AFM height contrast, (b) AFM height image after shear and UV treatment, with inset showing the height profile taken along the white line to the left of the inset, (c) AFM height image after deposition and shear of the second layer without UV treatment, (d) SEM image after O_2 RIE with inset showing Fourier transform, and (e) same at high magnification. Panel (f) shows an SEM image of a similar bilayer film after O_2 RIE, but wherein the second shear was applied at a 45° angle to the first shear, instead of 90°, to create a rhombic pattern. Scale bars are 500 nm in panels (a–d) and 100 nm in panels (e,f).

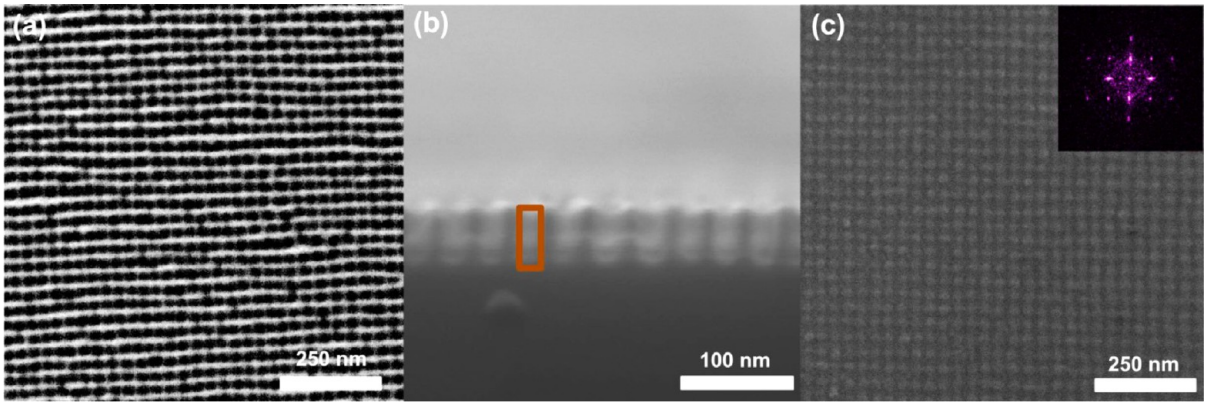

Figure 2. SEM images showing (a) top view of square array of nanowells, (b) cross-sectional view of the same nanowell array with the orange rectangle outlining the vertical cross-section of the "bore" of one of the wells (55 nm deep, 20 nm across), and (c) square array of PFS-residue posts created by controlled wet etching of the bilayer template prepared by O_2 RIE (step g in Scheme 1) with the Fourier transform shown in the inset.

alignment, the majority PS block was cross-linked using UV irradiation, thereby fixing the structure (step b in Scheme 1). Figure 1b shows the AFM height image after UV cross-linking; a modest amount of UV-induced degradation of the PS accompanies cross-linking, enhancing the weak height contrast evident by AFM prior to irradiation. A second uniform monolayer of PS-PFiPMS 36-15 (19 nm thick) was then spin-coated on top of the first layer, and the same shearing conditions were then applied to the bilayer film perpendicular to the first shear direction. Effective alignment of the second layer in the shear direction was confirmed with AFM as shown in Figure 1c. Note that cross-linking of the first layer allows the orientation of the cylinders in the different layers to be set independently in the two separate shearing steps; otherwise, the cylinder orientations and positions in the two layers would be strongly coupled.[30] Previously, such decoupling has been achieved only through prior conversion of the first layer to an inorganic residue by plasma etching[29] or by the deposition of dense silicon membranes (~10 nm thick) between the layers.[31]

dx.doi.org/10.1021/nl502416b | *Nano Lett.* 2014, 14, 5698–5705

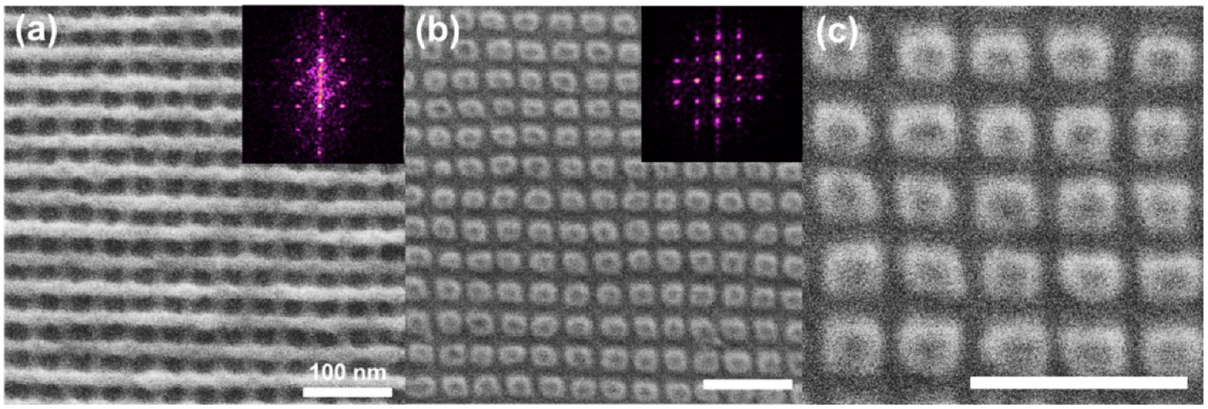

Figure 3. SEM images of (a) etched bilayer template after evaporation of 3 nm Cr, prior to PFS residue removal, (b,c) Cr dot array after lift-off at two different magnifications. All scale bars indicate 100 nm. Insets in (a,b) show the Fourier transforms of the images, indicating highly ordered arrays with square packing.

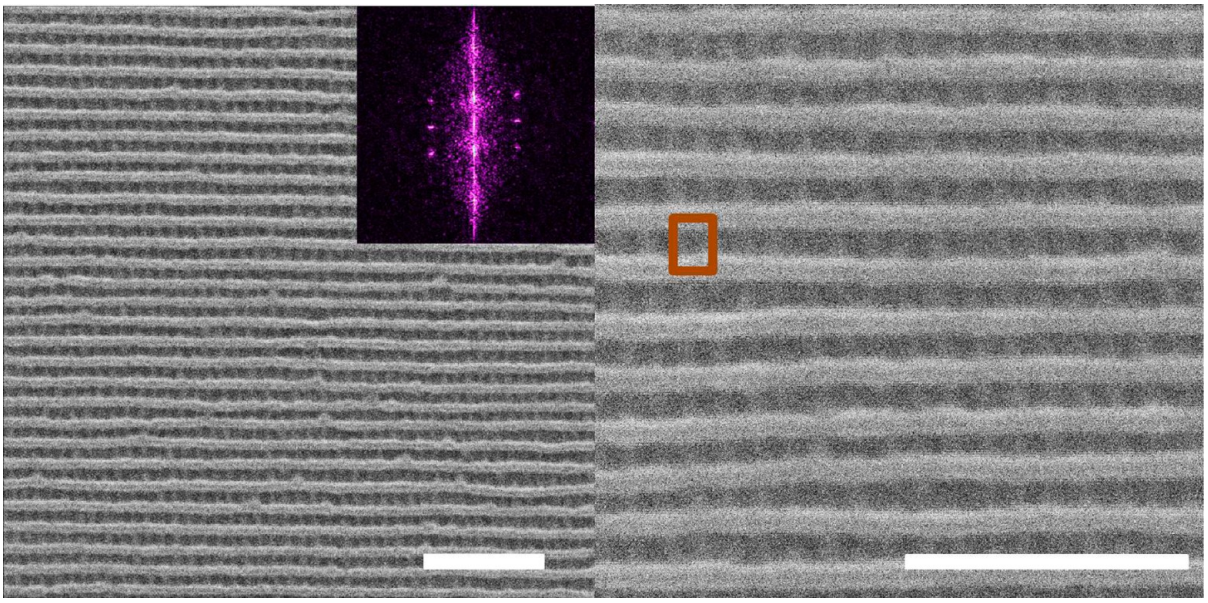

Figure 4. SEM images, taken at two different magnifications, of rectangular patterns created from PS-PFEMS 27-11 (bottom layer, 23 nm periodicity, shear direction vertical) and PS-PFiPMS 36-15 (top layer, 35 nm periodicity, shear direction horizontal). The inset in the left image shows the Fourier transform of the array (aspect ratio 1.57), while the orange inset in the right image outlines the rectangular unit cell of the array. Both scale bars represent 200 nm.

To reveal the structure of both layers, the PS matrix of the bilayer film was selectively removed via oxygen (O_2) RIE; polyferrocenylalkylsilanes (PFS) are strongly resistant to O_2 RIE due to the iron and silicon they contain, while the all-organic PS blocks are completely removed.[32,33] Figure 1d,e shows scanning electron microscopy (SEM) images of the square patterns formed by the PFS residue remaining after O_2 RIE; the pitch of the nanosquare grid is 35 nm, set by the intercylinder spacing of the PS-PFiPMS 36-15. The lines constituting the grid each have a width of 14 ± 3 nm after etching. This uniform square pattern was observed over the entire area (>1 cm^2) underneath the pad used to apply the shear stress with long-range order and a low defect density; for example, no dislocations are visible in Figure 1d (2 μm^2 area). While occasional isolated dislocations were observed in other images of grids derived from PS-PFiPMS 36-15, their areal density averaged well below 1 dislocation/μm^2, in contrast with the values of 1−4 dislocations/μm^2 reported in other well-ordered shear-aligned block copolymers.[25]

In the preceding example, the second shear stress was applied at a 90° angle to the first shear stress to produce square arrays; however, the angle between the two shear stresses can be continuously tuned, yielding rhombic patterns of any desired angle.[29] Figure 1f shows a rhombic array created from a PS-PFiPMS 36-15 bilayer film, where the shear directions differ by 45° between the two layers, rather than 90°.

Etched bilayer films such as those shown in Figure 1e,f can serve as templates for patterned arrays with several different types of elements. For example, the strong etch resistance of PFS not only to O_2 RIE but also to SF_6 RIE allows the pattern to be transferred into other substrates (e.g., silicon) via the Bosch process,[34] creating nanosquare wells (step f in Scheme 1) as shown in the SEM image in Figure 2a. Wells 55 nm deep were created in this example, as measured from cross-sectional SEM images of the grids as shown in Figure 2b; with this etching protocol and polymer, the depth of the wells could reach 80 nm.[26] Such nanosquare wells could potentially be used

dx.doi.org/10.1021/nl502416b | Nano Lett. 2014, 14, 5698−5705

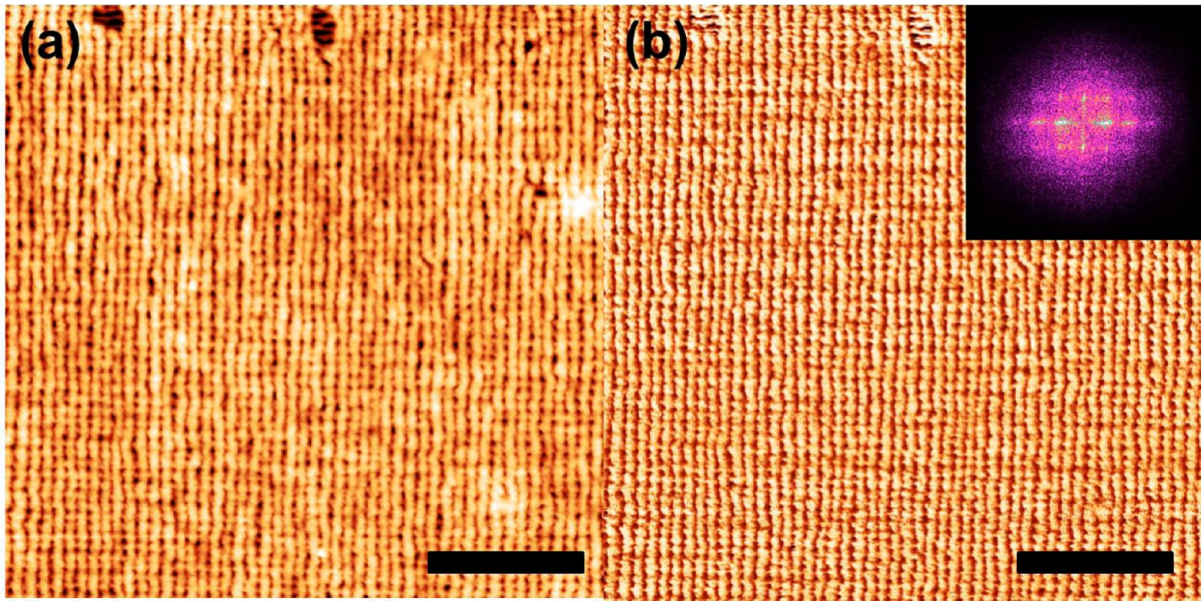

Figure 5. Tapping-mode AFM images of a PS-PHMA 33-78 bilayer film after removal of the PHMA matrix by UV irradiation for 3 min and rinsing with toluene: (a) height and (b) phase images. Inset shows the Fourier transform of the phase image, again revealing a well-ordered square array. Scale bar indicates 500 nm.

to contain individual proteins or other biomolecules, or as a master mold for nanoimprint lithography.

While the PFS residue is highly resistant to RIE, it is amenable to wet etching by acids. The cross-points in the bilayer structure are slowest to etch, so judicious control of the etch time in 5% HCl (aq) with sonication yields a square array of nanoposts (step g in Scheme 1), as shown by the SEM image in Figure 2c. The strong RIE etch resistance of the PFS residue forming these dots could permit further pattern transfer into the substrate, such as via the Bosch etch process employed in the preceding example, to generate the inverse structure (tall Si nanoposts vs deep nanowells in Si).

Next, we show that these same cross-bar templates can be used to fabricate highly ordered square arrays of metal nanodots (step h in Scheme 1); metal nanodots are of interest for high density magnetic storage[10,35,36] and plasmonics.[37] Previous work has employed block copolymer templates to fabricate high-density metal dot arrays,[10,35,38−40] even large-area arrays possessing long-range order, using a shear-aligned template,[40] but diblock copolymers self-assemble into hexagonal, not square, arrays. Here, we used the cross-bar template obtained after O_2 RIE to create metal dots (step h in Scheme 1) by evaporating 3 nm of chromium (Cr) over the template (Figure 3a), then removing the excess Cr and the PFS residue by sonication in 5% HCl (aq). A square array of Cr dots with low defect density was obtained, as shown in Figure 3b. The center-to-center distance of the dots remains at 35 nm, which was the intercylinder spacing in each layer of the bilayer template; the individual dots have a square shape, ∼25 nm on a side and with relatively sharp corners (radius of curvature typically <5 nm). The dot array covers the entire cm^2 area where shear alignment was imparted to the film; to the best of our knowledge, these are the first metal nanodots fabricated in square arrays via block copolymer templating.

Because the periodicity of the stripe pattern is determined by the block copolymer molecular weight,[24] the size and spacing of the nanodots are readily controlled by using block copolymers of different molecular weight. Furthermore, since the layers in the film are deposited and sheared individually, there is no need for the same polymer to be employed for the different layers; if the intercylinder periodicity is different between the two layers, a rectangular array should result. As an example, a cylinder-forming polystyrene-*b*-poly(ferrocenylethylmethylsilane), PS-PFEMS 27-11, was employed for the first layer (18 nm thick) with a number-average molecular weight M_n = 38 kg/mol, yielding a 23 nm intercylinder periodicity; for the second layer (19 nm thick), PS-PFiPMS 36-15 with a hemicylinder periodicity of 35 nm was again used. After O_2 RIE, highly regular rectangular grids are obtained as shown in Figure 4 with an aspect ratio of 1.57 (±0.01, 1 standard deviation) measured from the spots in the Fourier transform, which is in good agreement with the ratio of the intercylinder spacings in monolayers of the individual block copolymers (35 nm/23 nm = 1.52 ± 0.04). The cross-bar pattern of Figure 4 in turn could be used as a template for rectangular arrays of metal nanodots, following step h of Scheme 1.

While the preceding examples relied upon the excellent dry etch resistance of PFS blocks, both to create the cross-bar template and to effect pattern transfer into the substrate, the approach presented here is not limited to block copolymers containing PFS. The requirements are simply that at least one of the blocks is cross-linkable without extensive degradation of the film and that the matrix block is selectively removable under conditions that do not significantly deform the cylindrical domains (e.g., dry etching, or wet etching in a nonsolvent). As an example of an all-organic chemistry, the same bilayer structure illustrated in Scheme 1a−e was fabricated from a polystyrene-poly(*n*-hexyl methacrylate) diblock, PS-PHMA 33-78, which forms full PS cylinders parallel to the substrate with an intercylinder spacing of 40 nm in a film 35 nm thick (see Supporting Information, Figure S3). The UV irradiation used to cross-link the PS block also partially degrades the PHMA matrix (Supporting Information, Figure S3b); degraded material was removed by rinsing with toluene. A second layer of PS-PHMA 33-78 (35 nm thick) was spin-coated on top of the first layer and sheared perpendicular to the first direction.

dx.doi.org/10.1021/nl502416b | *Nano Lett.* 2014, 14, 5698−5705

Prior to application of the second shear, the UV-induced topography of the first layer produces an alignment of the cylinders in the second layer that generally follows that in the first layer, albeit with a very high density of defects (inset to Supporting Information, Figure S3c); this orientation is completely eliminated by the second shear. Further UV irradiation of the bilayer degrades the PHMA matrix in both layers; rinsing with toluene reveals the cross-stacked PS cylinders, as shown in Figure 5. The bottom layer of lines in the cross-bar pattern (horizontal in Figure 5) is difficult to resolve by AFM, because these lie at the bottom of the "channels" formed by the top (vertical) layer of the cross-bar array; however, their presence is clearly evident in the Fourier transform shown as the inset in Figure 5b. Note that in this example, the minority block (PS) is cross-linked, while in the previous PS-PFS examples it was the matrix block (also PS) that was cross-linked; further, in the previous examples, PS was the rapidly etched block (with O_2 RIE), while in the present example, PS is the etch-resistant block (to UV irradiation). However, extensive exposure to UV irradiation also degrades PS, so the UV irradiation time must be properly controlled.

Alternatively, O_2 or CF_4 RIE can be employed to selectively remove the PHMA matrix, as both gases etch PHMA twice as fast as PS;[41] an SEM image of a square array formed from a PS-PHMA 33-78 bilayer after CF_4 RIE is shown in Supporting Information, Figure S4. A rhombic array was also prepared from PS-PHMA 33-78 with a 70° angle between the cylinder axes in the two layers (Supporting Information, Figure S5), again demonstrating the continuously tunable nature of the layer alignment directions.

To sum up, we have introduced a simple, fast and inexpensive method to create square, rectangular, and rhombic nanoscale patterns over macroscopic (cm^2) areas with the pattern symmetry easily adjusted through the molecular weights of the block copolymers (rectangular versus square) and through the independently set shear directions for the two layers (square versus rhombic). Further, we have demonstrated transfer of these patterns into nanowells, nanoposts, and metal nanodots. The only requirement regarding the chemistry of the block copolymer layers appears to be that they should be cross-linkable without extensive degradation, as in the cross-linking of PS by UV irradiation employed here. Because the structure and orientation of each layer is set independently and fixed by cross-linking, the method could in the future be extended to stacks containing layers with different morphologies: for instance, stripe patterns from shear-aligned cylinders or perpendicular lamellae[42] in the bottom layer and an oriented hexagonal lattice from a shear-aligned sphere-forming block copolymer[40] in the top layer.

Experimental Methods. *Materials.* Silicon wafers were purchased from Silicon Quest International and used without further cleaning. Polystyrene-*block*-poly(ferrocenylisopropylmethylsilane), PS-PFiPMS 36-15, with a number-average molecular weight M_n = 51 kg/mol, dispersity $Đ$ = 1.09, and weight fraction of PFiPMS w_{PFS} = 0.30 (volume fraction of cylinders φ = 0.26) was synthesized by sequential living anionic polymerization.[43] Polystyrene-*block*-poly(ferrocenylethylmethylsilane), PS-PFEMS 27-11, with M_n = 38 kg/mol, $Đ$ = 1.07, and w_{PFS} = 0.30 (φ_{PFS} = 0.26) was synthesized by click-coupling of alkyne end-functionalized PS and azide end-functionalized PFEMS, each of which was synthesized by living anionic polymerization with functional termination (see Supporting Information for details). Poly(styrene)-*block*-poly(*n*-hexyl methacrylate), PS-PHMA 33-78, with M_n = 111 kg/mol, $Đ$ = 1.06, and PS weight fraction w_{PS} = 0.30 (φ_{PS} = 0.29) was synthesized via sequential living anionic polymerization.[44] Volume fractions were calculated from weight fractions using room-temperature densities of 1.05 g/cm^3 for PS,[45] 1.01 g/cm^3 for PHMA,[45] 1.29 g/cm^3 for PFEMS,[46] and 1.26 g/cm^3 for PFiPMS.[43] Hydroxyl-terminated PS with M_n = 51 kg/mol and $Đ$ = 1.03 was purchased from Polymer Source, Inc.

Shear Alignment. Cross-linked poly(dimethylsiloxane), PDMS, sheets approximately 0.6 mm thick were prepared from Sylgard 184 (Dow Corning) at a 10:1 weight ratio of PDMS base/curing agent and cured at 60 °C for 24h. Pads measuring 1.3 × 1.3 cm^2 were cut from these sheets. For PS-PFS shear alignment, uncross-linked PDMS oligomers were removed from the pads by soaking in triethylamine for 24 h,[47] followed by sequential rinsing with acetone and isopropanol and drying; this extraction was necessary to achieve the best pattern transfer, as PDMS oligomers will also leave a residue after O_2 RIE. Pads were placed on top of the block copolymer-coated substrates for shear alignment, as described previously;[5] 780 g of normal force and 300 g of shear force (shear stress = 17 kPa) were applied for 30 min while holding the film at 150 °C, well above the glass transition temperatures of both blocks ($T_{g,PS}$ ~100 °C, $T_{g,PFiPMS}$ ~ 60 °C, $T_{g,PFEMS}$ ~ 25 °C, and $T_{g,PHMA}$ ~ −5 °C). For the rectangular-shaped patterns employing PS-PFEMS 27-11 as the bottom layer, hydroxyl-terminated PS was spin-coated at 40 nm thickness and annealed at 170 °C in vacuum for 23 h for grafting. Ungrafted polymer was removed by repeated rinsing with toluene, yielding a final grafted thickness of 8 nm. As discussed further in the Supporting Information, PS-PFEMS exhibits asymmetric wetting behavior (Supporting Information, Figure S1); the grafted PS layer eliminates the etch-resistant PFEMS layer which PS-PFEMS 27-11 would otherwise deposit at the substrate and produces a layer of full cylinders in a PS-PFEMS 27-11 film which is 18 nm thick (Supporting Information, Figure S2).

UV Irradiation and Etching. After shear alignment of the first layer, the specimen was irradiated with a UV light source (Light Sources 8354L lamp, driven at 420 mA, 5 cm from lamp to specimen) in air for 4 min for PS-PFiPMS 36-15 and PS-PFEMS 27-11 or 1 min for PS-PHMA 33-78. The optimum UV exposure time for cross-linking of the first layer was determined from a series of measurements on PS homopolymer films, as the time at which the film thickness after exposure was least changed by rinsing with toluene, indicating both good cross-linking and minimal chain fragmentation of PS. After UV irradiation and rinsing with toluene, a PS-PFiPMS 36-15 monolayer (19 nm thick) decreased in thickness by only 3 nm, while the PS-PHMA 33-78 monolayer (34 nm) lost 12 nm of thickness. To remove the PS matrix in PS-PFS bilayers, O_2 RIE was performed with either a Plasmatherm 790 using 10 sccm of O_2 at a pressure of 15 mTorr and a power density of 0.24 W/cm^2, for 55 s, or a Technics Planaretch II at 5 sccm, 0.2 Torr, and 47 W for 45 s. For selected PS-PHMA 33-78 bilayer samples, as in Supporting Information, Figure S2, matrix removal was achieved by exposure to UV for 1 min after the second shear, followed by CF_4 RIE for 11 s (Plasmatherm 790) at the same conditions described above.

Bosch Etching. Pattern transfer from the etched PS-PFiPMS 36-15 bilayer into the silicon substrate was realized via Bosch etching, performed with a SAMCO 800 at 100 W ICP power

dx.doi.org/10.1021/nl502416b | Nano Lett. 2014, 14, 5698−5705

and 50 W bias. The procedure was optimized[26] for the small feature sizes present in the block copolymer templates: for the first 5 cycles, the flow rates of SF_6, C_4F_8, and O_2 were 30, 50, and 2 sccm with a period of 2 s, equally split between SF_6 and C_4F_8/O_2, while for the next 8 cycles, the period was increased to 4 s, and the flow rates of SF_6 and C_4F_8 were decreased to 20 and 35 sccm, respectively.

Metal Evaporation and Lift-off. Deposition of 3 nm of Cr was done with a Denton/DV-502A electron beam evaporator at $<10^{-6}$ Torr. Lift-off of excess Cr from the etched PS-PFiPMS 36-15 bilayer was achieved by immersing in 5% HCl (aq) solution for 24 h with occasional sonication, followed by rinsing with deionized water.

Characterization. Polymer film thicknesses were measured using ellipsometry at 632.8 nm (Gaertner Scientific LS116S300). Imaging of the block copolymer films and nanogrids employed high-resolution SEM (FEI Quanta 200 Environmental SEM, high-vacuum mode, 15 keV, secondary electron images) and tapping-mode AFM (Digital Instruments Dimension 3000, 1.9 Hz scan rate, using NanoWorld FM tips operating at 75 kHz resonance). Cross-sectional SEM images were obtained by cleaving the wafer perpendicular to the shear-alignment direction with a diamond cutter.

■ ASSOCIATED CONTENT

Supporting Information

Details of the synthesis of PS-PFEMS 27-11; determination of the asymmetric wetting behavior exhibited by PS-PFEMS 27-11; SEM image of a uniform, shear-aligned monolayer of PS-PFEMS 27-11 on a PS-grafted substrate; AFM images of PS-PHMA 33-78 films at various steps in the process flow leading to Figure 5; SEM image of PS-PHMA 33-78 bilayer film after CF_4 RIE; AFM image of PS-PHMA 33-78 bilayer forming a rhombic array. This material is available free of charge via the Internet at http://pubs.acs.org.

■ AUTHOR INFORMATION

Corresponding Author

*E-mail: register@princeton.edu.

Notes

The authors declare no competing financial interest.

■ ACKNOWLEDGMENTS

This work was supported by the National Science Foundation (MRSEC Program) through the Princeton Center for Complex Materials (DMR-0819860). We gratefully acknowledge Dr. Jia Gao for helpful discussions on metal evaporation.

■ REFERENCES

(1) Gu, X.; Gunkel, I.; Russell, T. P. *Philos. Trans. R. Soc. London, Ser. A* **2013**, *370*, 20120306.
(2) Stoykovich, M. P.; Nealey, P. F. *Mater. Today* **2006**, *9*, 20−29.
(3) Kim, H. C.; Park, S. M.; Hinsberg, W. D. *Chem. Rev.* **2010**, *110*, 146−177.
(4) Marencic, A. P.; Register, R. A. *Annu. Rev. Chem. Biomol. Eng.* **2010**, *1*, 277−297.
(5) Angelescu, D. E.; Waller, J. H.; Adamson, D. H.; Deshpande, P.; Chou, S. Y.; Register, R. A.; Chaikin, P. M. *Adv. Mater.* **2004**, *16*, 1736−1740.
(6) Li, R. R.; Dapkus, P. D.; Thompson, M. E.; Jeong, W. G.; Harrison, C.; Chaikin, P. M.; Register, R. A.; Adamson, D. H. *Appl. Phys. Lett.* **2000**, *76*, 1689−1691.
(7) Park, J. H.; Khandekar, A. A.; Park, S. M.; Mawst, L. J.; Kuech, T. F.; Nealey, P. F. *J. Cryst. Growth* **2006**, *297*, 283−288.
(8) Kuech, T. F.; Mawst, L. J. *J. Phys. D: Appl. Phys.* **2010**, *43*, 183001.
(9) Huang, Y.; Kim, T. W.; Xiong, S.; Mawst, L. J.; Kuech, T. F.; Nealey, P. F.; Dai, Y.; Wang, Z.; Guo, W.; Forbes, D.; Hubbard, S. M.; Nesnidal, M. *Nano Lett.* **2013**, *13*, 5979−5984.
(10) Naito, K.; Hieda, H.; Sakurai, M.; Kamata, Y.; Asakawa, K. *IEEE Trans. Magn.* **2002**, *38*, 1949−1951.
(11) Black, C. T.; Guarini, K. W.; Zhang, Y.; Kim, H. J.; Benedict, J.; Sikorski, E.; Babich, I. V.; Milkove, K. R. *IEEE Electron Device Lett.* **2004**, *25*, 622−624.
(12) Li, W. K.; Yang, S. *J. Vac. Sci. Technol., B* **2007**, *25*, 1982−1984.
(13) Stoykovich, M. P.; Kang, H.; Daoulas, K. C.; Liu, G.; Liu, C. C.; de Pablo, J. J.; Mueller, M.; Nealey, P. F. *ACS Nano* **2007**, *1*, 168−175.
(14) Hardy, C. G.; Tang, C. *J. Polym. Sci., Part B: Polym. Phys.* **2013**, *51*, 2−15.
(15) Mogi, Y.; Nomura, M.; Kotsuji, H.; Ohnishi, K.; Matsushita, Y.; Noda, I. *Macromolecules* **1994**, *27*, 6755−6760.
(16) Son, J. G.; Gwyther, J.; Chang, J.-B.; Berggren, K. K.; Manners, I.; Ross, C. A. *Nano Lett.* **2011**, *11*, 2849−2855.
(17) Tang, C. B.; Lennon, E. M.; Fredrickson, G. H.; Kramer, E. J.; Hawker, C. J. *Science* **2008**, *322*, 429−432.
(18) Park, S.-M.; Craig, G. S. W.; La, Y.-H.; Solak, H. H.; Nealey, P. F. *Macromolecules* **2007**, *40*, 5084−5094.
(19) Ji, S.; Nagpal, U.; Liao, W.; Liu, C.-C.; de Pablo, J. J.; Nealey, P. F. *Adv. Mater.* **2011**, *23*, 3692−3697.
(20) Tavakkoli, A. K. G.; Gotrik, K. W.; Hannon, A. F.; Alexander-Katz, A.; Ross, C. A.; Berggren, K. K. *Science* **2012**, *336*, 1294−1298.
(21) Amir Tavakkoli, K. G.; Nicaise, S. M.; Hannon, A. F.; Gotrik, K. W.; Alexander-Katz, A.; Ross, C. A.; Berggren, K. K. *Small* **2014**, *10*, 493−499.
(22) Ruiz, R.; Dobisz, E.; Albrecht, T. R. *ACS Nano* **2011**, *5*, 79−84.
(23) Wan, L.; Ruiz, R.; Gao, H.; Patel, K. C.; Lille, J.; Zeltzer, G.; Dobisz, E. A.; Bogdanov, A.; Nealey, P. F.; Albrecht, T. R. *J. Micro/Nanolithogr., MEMS, MOEMS* **2012**, *11*, 031405.
(24) Papalia, J. M.; Adamson, D. H.; Chaikin, P. M.; Register, R. A. *J. Appl. Phys.* **2010**, *107*, 084305.
(25) Marencic, A. P.; Chaikin, P. M.; Register, R. A. *Phys. Rev. E* **2012**, *86*, 021507.
(26) Kim, S. Y.; Gwyther, J.; Manners, I.; Chaikin, P. M.; Register, R. A. *Adv. Mater.* **2014**, *26*, 791−795.
(27) Singh, G.; Yager, K. G.; Berry, B.; Kim, H. C.; Karim, A. *ACS Nano* **2012**, *6*, 10335−10342.
(28) Qiang, Z.; Zhang, L. H.; Stein, G. E.; Cavicchi, K. A.; Vogt, B. D. *Macromolecules* **2014**, *47*, 1109−1116.
(29) Jeong, J. W.; Hur, Y. H.; Kim, H.-J.; Kim, J. M.; Park, W. I.; Kim, M. J.; Kim, B.; Jung, Y. S. *ACS Nano* **2013**, *7*, 6747−6757.
(30) Harrison, C.; Park, M.; Chaikin, P.; Register, R. A.; Adamson, D. H.; Yao, N. *Macromolecules* **1998**, *31*, 2185−2189.
(31) Rose, F.; Bosworth, J. K.; Dobisz, E. A.; Ruiz, R. *Nanotechnology* **2011**, *22*, 035603.
(32) Korczagin, I.; Lammertink, R. G. H.; Hempenius, M. A.; Golze, S.; Vancso, G. J. *Adv. Polym. Sci.* **2006**, *200*, 91−117.
(33) Nunns, A.; Gwyther, J.; Manners, I. *Polymer* **2013**, *54*, 1269−1284.
(34) Chang, C. L.; Wang, Y. F.; Kanamori, Y.; Shih, J. J.; Kawai, Y.; Lee, C. K.; Wu, K. C.; Esashi, M. *J. Micromech. Microeng.* **2005**, *15*, 580−585.
(35) Cheng, J. Y.; Ross, C. A.; Chan, V. Z. H.; Thomas, E. L.; Lammertink, R. G. H.; Vancso, G. J. *Adv. Mater.* **2001**, *13*, 1174−1178.
(36) Sun, S. H.; Murray, C. B.; Weller, D.; Folks, L.; Moser, A. *Science* **2000**, *287*, 1989−1992.
(37) Wang, Z. C.; Chumanov, G. *Adv. Mater.* **2003**, *15*, 1285−1289.
(38) Park, M.; Chaikin, P. M.; Register, R. A.; Adamson, D. H. *Appl. Phys. Lett.* **2001**, *79*, 257−259.
(39) Shin, K.; Leach, K. A.; Goldbach, J. T.; Kim, D. H.; Jho, J. Y.; Tuominen, M.; Hawker, C. J.; Russell, T. P. *Nano Lett.* **2002**, *2*, 933−936.
(40) Vedrine, J.; Hong, Y.-R.; Marencic, A. P.; Register, R. A.; Adamson, D. H.; Chaikin, P. M. *Appl. Phys. Lett.* **2007**, *91*, 143110.

(41) Pelletier, V.; Asakawa, K.; Wu, M.; Adamson, D. H.; Register, R. A.; Chaikin, P. M. *Appl. Phys. Lett.* **2006**, *88*, 211114.
(42) Pujari, S.; Keaton, M. A.; Chaikin, P. M.; Register, R. A. *Soft Matter* **2012**, *8*, 5358−5363.
(43) Gwyther, J.; Manners, I. *Polymer* **2009**, *50*, 5384−5389.
(44) Kwon, H.-K.; Lopez, V. E.; Davis, R. L.; Kim, S. Y.; Burns, A. B.; Register, R. A. *Polymer* **2014**, *55*, 2059−2067.
(45) Zoller, P.; Walsh, D. J. *Standard Pressure-Vol.-Temperature Data for Polymers*; Technomic Publishing: Lancaster, PA, 1995.
(46) Rider, D. A.; Cavicchi, K. A.; Power-Billard, K. N.; Russell, T. P.; Manners, I. *Macromolecules* **2005**, *38*, 6931−6938.
(47) Lee, J. N.; Park, C.; Whitesides, G. M. *Anal. Chem.* **2003**, *75*, 6544−6554.

dx.doi.org/10.1021/nl502416b | *Nano Lett.* 2014, 14, 5698−5705